Journal of Power Sources 340 (2017) 71–79

Contents lists available at ScienceDirect

Journal of Power Sources

journal homepage: www.elsevier.com/locate/jpowsour

Energy efficiency of a concentration gradient flow battery at elevated temperatures

W.J. van Egmond [a, b, *], U.K. Starke [b], M. Saakes [b], C.J.N. Buisman [a, b], H.V.M. Hamelers [b]

[a] Department of Environmental Technology, Wageningen University, Bornse Weilanden 9, 6708 WG, Wageningen, The Netherlands
[b] Wetsus, European Centre of Excellence for Sustainable Water Technology, Oostergoweg 9, 8911 MA, Leeuwarden, The Netherlands

HIGHLIGHTS

- A Concentration Gradient Flow Battery (CGFB) is operated at elevated temperatures.
- Instantaneous mass transport and (dis)charge efficiency of a CGFB is analysed.
- An efficient operating range with maximum depth of discharge for a GCFB is identified.
- Water transport causes hysteresis and a decrease in energy capacity and efficiency.
- At increasing temperatures osmosis increases but electro-osmosis is unaffected.

GRAPHICAL ABSTRACT

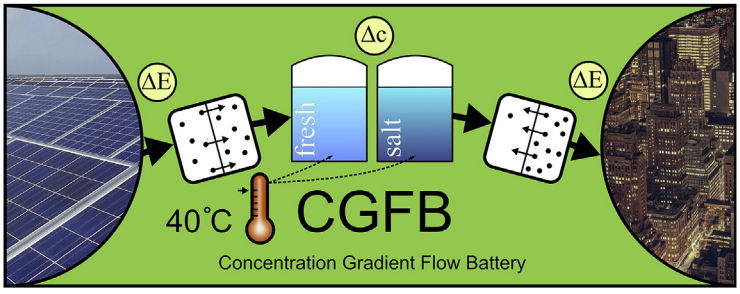

ARTICLE INFO

Article history:
Received 19 July 2016
Received in revised form
7 October 2016
Accepted 11 November 2016
Available online 22 November 2016

Keywords:
Concentration gradient flow battery
Large scale electricity energy storage
Stationary batteries
Reverse electrodialysis
Charge/discharge efficiency
Aqueous electrolyte

ABSTRACT

Fast growth of intermittent renewable energy generation introduces a need for large scale electricity storage. The Concentration Gradient Flow Battery (CGFB) is an emerging technology which combines Electrodialysis with Reverse Electrodialysis into a flow battery which is able to safely store very large amounts of energy in environmental friendly NaCl solutions. In this work, (dis)charge efficiency, energy density and power density are both theoretically and experimentally investigated. Fifteen constant current experiments (−47.5 to +37.5 A m^{-2}) are performed at 40 °C and two experiments (−32.5 and 15 A m^{-2}) at 10 and 25 °C. The magnitudes of the three main energy dissipation sources (internal resistance, water transport and co-ion transport) are measured and mitigation strategies are proposed. The effect of current density, state of charge and temperature on the dissipation sources is analysed. Water transport is shown to cause hysteresis, lower (dis)charge efficiencies and lower energy capacity. At constant current and with increasing temperature, internal resistance is reduced but unwanted water transport is increased. This study reports charge efficiencies up to 58% and discharge efficiencies up to 72%. Full charge or discharge of the battery is shown inefficient. The optimal operating range is therefore introduced and identified (concentration difference $\Delta m > 0.5$ and energy efficiency $\eta > 0.4$).

1. Introduction

Production of renewable energy and the necessity to balance electricity production and consumption are driving development of

* Corresponding author. Department of Environmental Technology, Wageningen University, PO Box 17, 6700 AA, Wageningen, The Netherlands.
E-mail address: janwillem.vanegmond@wetsus.nl (W.J. van Egmond).

http://dx.doi.org/10.1016/j.jpowsour.2016.11.043

various types of energy storage systems [1–5]. One of the main challenges in this area is the required capacities of large scale electrical energy storage (EES) systems in the electricity grid. Recently, a concentration gradient flow battery (CGFB) was proposed as an environmental friendly EES system [6,7]. A CGFB stores energy in two reservoirs filled with aqueous solutions of different salinity. This system stores power in two solutions with different concentrations using the Electro Dialysis (ED) process [8–11]. The reverse process, Reverse Electro Dialysis (RED), must be carried out in order to discharge the CGFB [12–14]. The resulting battery is scalable, can be placed anywhere in the world and uses abundant materials only.

Fig. 1 shows the concept of the CGFB during charging mode (ED mode). A completely discharged CGFB constitutes two aqueous reservoirs containing solutions with equal salt concentration, a so called 'stack' of alternately placed cation and anion exchange membranes and pumps. Both solutions are pumped through the stack and returned to their respective reservoir. The membranes contain fixed charges (represented schematically in Fig. 1 by + and − signs) which makes the membranes ion-selective. Cation exchange membranes allow cations to pass and block anions and anion exchange membranes allow anions to pass while blocking cations. An electric potential is applied over the outer electrodes (black bars) during charging. As a result, ions will move across the membranes in one stream becoming more concentrated (c,out) and one stream more diluted (d,out). In this way electric power is spent for creating one concentrated reservoir (salt) and one diluted reservoir (fresh). To discharge the CGFB, the current direction is reversed. Ions move in opposite direction and the solutions mix under the influence of a concentration difference over the membranes. Power is harvested over the outer electrodes while the salinity difference decreases. Ionic current over the membranes needs to be converted to electric current at the electrodes. For this, redox reactions at the electrodes in a secondary solution take place. The secondary solution is circulated in a separated closed loop. In a true sized GCFB, any energy loss as result of the redox reaction is negligible. Therefore, these losses are excluded from this study.

In the charge/discharge process, all mass transport takes place through the membranes. Three dissipation factors decrease the (dis)charge efficiency: internal resistance, water transport and co-ion transport [7]. Internal resistance is the result of the electric resistance over the membranes and solution compartments. Water transport consists of osmosis and electro-osmosis. Osmosis occurs over the membrane as a result of a concentration difference and always constitutes a potential energy loss since it decreases the salinity difference without harvesting power. Electro-osmosis is water transport as a result of water associated with ions in their mantle. Depending on the direction of ion transport, associated water can be transported against or along the concentration gradient. Co-ion transport refers to unwanted ion transport as result of diffusion over membranes because membranes are not perfectly charge selective.

Initial studies on CGFB performance [6,7] show that the (dis) charge efficiency and power density of such systems are rather limited due to internal resistance and osmosis (<40% round trip efficiency). Reduction of internal resistance is therefore a straightforward solution for increasing both (dis)charge efficiency and power density of a CGFB. Earlier work on RED and ED shows that the internal resistance can be significantly reduced by increasing operating temperatures [15–21]. This study investigates experimentally how operating a CGFB at different current densities and at an elevated temperature of 40 °C affects instantaneous system internal resistance, mass transport, (dis)charge efficiency and energy density over complete charge/discharge cycles. It also points out "hysteresis" of a CGFB, which is a result of water transport through the membranes from the fresh solution to concentrate solution preventing the battery from returning to its original state. In this work, the working range of salt concentration is limited to 1 M NaCl, because operating the CGFB above that value leads to excessive energy losses due to osmotic water transport [7]. Finally, an accurate mass transport measurement method is presented as well.

2. Theory of a CGFB

In this section, theory of a CGFB is presented. Important equations for energy density, mass transport and (dis)charge efficiency calculation are given and explained.

2.1. Energy density

Gibbs free energy of mixing becomes available when two solutions of different salinity mix inside a CGFB. The theoretical amount of energy ΔG_{mix} (J) that can be released during this process can be calculated according to

$$\Delta G_{mix} = G_{c,out} + G_{d,out} - G_{c,in} - G_{d,in} \quad (1)$$

$$G_i = n_w \nu m R T \left(\ln(\gamma_{\pm} m) - \phi\right) \quad (2)$$

where G_i is the total Gibbs energy of a solution i, n_w the number of kilograms of solvent, ν the number of types of ions in a solution, m the molality of a solution, R the universal gas constant, T temperature, ϕ the osmotic coefficient and $\gamma_{\pm}$ the mean molal activity coefficient. The subscripts on the right hand side of Eq. (1) refer to the concentrate and dilute solutions flowing either in or out a CGFB.

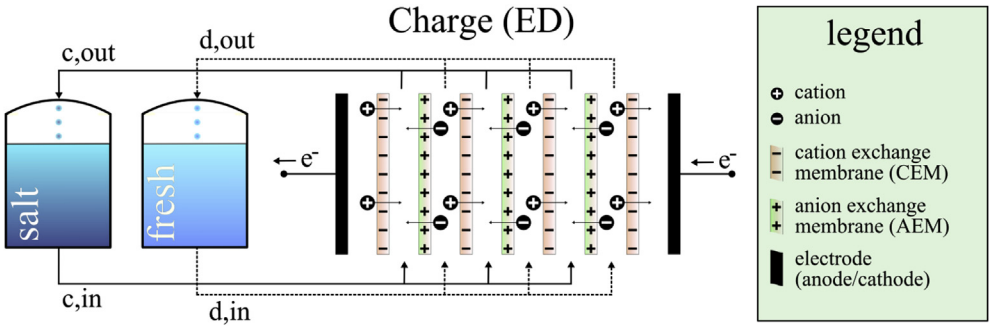

Fig. 1. Conceptual drawing of a CGFB during a charging step. Two reservoirs on the left contain two solutions of different salinity (salt and fresh). The solutions coming out the concentrated (salt) reservoir (c,in) and the diluted (fresh) reservoir (d,in) are pumped into the ED/RED stack. An electric potential is applied over the electrodes and ions will move across the membranes resulting in a more concentrated solution (c,out) and more diluted concentration (d,out) leading to an increase in salinity difference between the reservoirs.

The osmotic and molal activity coefficients are a function of salt concentration and temperature. In this work the approach of Pitzer et al. [22] and Silvester et al. [23] is used for calculating the coefficients at different temperatures.

2.2. Mass transport

In RED/ED there are 4 mass transport processes considered taking place across ion-exchange membranes [7,10,24,25]; (i) counter ion transport J_c, (ii) co-ion transport J_a, (iii) water osmosis J_{osm} and (iv) water electro-osmosis $J_{e\text{-}osm}$. Co-ion transport (or unwanted salt transport) is caused by a concentration and potential gradient across a membrane. This type of salt transport typically constitutes a loss in (dis)charge efficiency, since it decreases the concentration gradient. Osmotic water transport also contributes to lower (dis)charge efficiency, since it reduces the concentration gradient. Electro-osmotic water transport contributes to lower charge efficiency (ED mode), because it reduces the concentration gradient (as water is transported with ions from the diluate to concentrate solution). With RED mode, electro-osmotic water transport increases discharge efficiency, because it increases the concentration gradient. This is a result of ion transport taking place in reversed direction.

There are two types of membranes in a GCFB. This study assumes both membrane types have the same properties, except for the sign of fixed chemical charge. Based on this assumption, any mass transport process which occurs across a cation exchange membrane (CEM) is therefore mirrored in an adjacent anion exchange membrane (AEM). Together both membranes constitute a cell pair.

Charge transport across an ion-exchange membrane and salt transport across a cell pair can be described respectively by Ref. [7]

$$I_{mol} = J_c - J_a \tag{3}$$

$$J_s = J_c + J_a \tag{4}$$

The molar current density I_{mol} (mol ionic charge m^{-2} s^{-1} membrane) is the difference between counter ion and co-ion flux across a membrane and is calculated by dividing current density I_d (A m^{-2}) by Faradays constant F. The net salt transport J_s (mols of salt m^{-2} s^{-1}) represents the total amount of moles of salt transported across a cell pair.

Total water transport J_w (kg of H_2O m^2 s^{-1}) across a cell pair can be calculated according to

$$J_w = \overbrace{2L_p(-\Delta\mu_w)}^{osmosis} + \overbrace{J_s t_w M}^{electro-osmosis} \tag{5}$$

where L_p is the average water permeability coefficient (kg m^{-2} s^{-1} kg J^{-1}) of both membrane types and $\Delta\mu_w$ the difference in chemical potential of the water (J kg^{-1}) [7] over the two sides of a membrane. The amount of water associated with transported ions across a membrane is expressed as t_w (mol of H_2O per mol of salt) and is referred to as electro-osmosis coefficient.

2.3. Power dissipation and (dis)charge efficiency

The amount of Gibbs free energy stored or released per second in or from the solutions, P_G (Gibbs power, J s^{-1} m^{-2} cell pair), is calculated by

$$P_G = J_w(-\Delta\mu_w) + J_s(-\Delta\mu_s) \tag{6}$$

where $\Delta\mu_s$ (J mol^{-1}) is the chemical potential difference of the salt of two solutions [7] separated by an ion-exchange membrane. A more detailed explanation on how to calculate water and salt chemical potential differences, $\Delta\mu_w$ and $\Delta\mu_s$, is provided in Ref. [7]. Next to co-ion and water transport (Section 2.2), internal resistance is also a major source of power dissipation. To discriminate the contributions of each dissipation factor in Gibbs power, Eq. (6) can be split up into

$$P_G = \overbrace{J_w(-\Delta\mu_w)}^{water\ transport} + \overbrace{J_a(-\Delta\mu_s)}^{co-ion\ transport} + \overbrace{J_c(-\Delta\mu_s) - I_d E_{cell}}^{internal\ resistance} + \overbrace{I_d E_{cell}}^{cell\ power} \tag{7}$$

where P_G is the amount of Gibbs free energy stored (ED mode) in solution or Gibbs free energy released (RED mode) from solution per second. Cell power P_{cell} is the amount of electric power spent (ED mode) or electric power extracted (RED mode). Counter ion and co-ion transport, J_c and J_a can be calculated from combining Eqs. (3) and (4).

The discharge efficiency is defined as the ratio of electric power harvested over released Gibbs power, see Eq. (8). The charge efficiency is given by the ratio of Gibbs power stored over electric power spent during charging, see Eq. (9).

$$\eta_{RED} = \frac{P_{cell}}{P_G} \tag{8}$$

$$\eta_{ED} = \frac{P_G}{P_{cell}} \tag{9}$$

3. Experimental

3.1. Experimental setup

The experimental setup used in this study consists of a RED/ED stack, three peristaltic pumps, three reservoirs, three thermostatic baths, four conductivity meters, four pressure meters, two mass balances and a galvanostat. The stack is comparable to the one used in Ref. [26]. Inside the RED/ED stack four cation exchange membranes and three anion exchange membranes (CMX and AMX, Astom Corporation, Japan) are alternately placed between two endplates. Metal bolts were used to make the stack watertight. Between each membrane a silicone gasket with a thickness of 200 μm and spacer (Sefar AG, Switzerland) with a thickness of 180 μm and an open area of ~50% is placed. The endplates contain two titanium mesh electrodes coated with Ir/Ru (Magneto Special Anodes B.V., the Netherlands). The two salt water reservoirs are 500 ml glass bottles encapsulated by insulating foil. Both water reservoirs are placed on a mass balance connected to a computer which logs the mass. The rinse solution reservoir is a 1000 ml glass bottle, also encapsulated with insulating foil. All three reservoirs are separately connected to three dedicated thermostatic baths with spiral coils inside to control the temperature of all solutions. Two peristaltic pumps pump the salt water solutions sequentially through the spiral coils inside the thermostatic baths, separate pressure meters (Cerabar M, Endress+Hauser, Germany), conductivity meters (VERSA STAR, Thermo Fisher Scientific, USA), the RED/ED stack and another set of identical type of conductivity meters back to the bottles. Conductivity data is logged by a computer. The rinse solution is pumped by a separate peristaltic pump with two pump heads (one for the anode and another for the cathode compartment) sequentially through two pressure meters, through the RED/ED stack electrode compartments back to the bottle. To avoid any parasitic short-circuit currents, additional tubing is used

before and after the RED/ED stack. In addition, tubing is insulated with foil to keep the temperature as constant as possible. Any change in temperature of each solution due to travelling from the thermostatic bath to the stack, is taken into account by careful adjustment of the temperature inside the thermostatic bath. This ensures that the temperature of each solution inside the stack is correct during experiments. The galvanostat (Ivium Technologies, the Netherlands) is used to control current and measure potential across the RED/ED stack. Two reference electrodes (QM711X, QIS, the Netherlands) are placed in the electrode compartments in the middle of the endplates. The salt water solutions are prepared using NaCl of 99.5% purity (ESCO, the Netherlands) and the rinse solutions are prepared with laboratory grade Na_2SO_4 (VWR, the Netherlands). All water used in this work is demineralized.

3.2. Experimental procedure

In total, fifteen constant current ED and RED experiments are performed with solutions being recycled continuously. Six ED experiments at 40 °C are performed at current densities ranging from −10 A m^{-2} to −47.5 A m^{-2} with steps of −7.5 A m^{-2} first. Salt water bottles are filled with 250 g of 0.5 molal NaCl solutions at the beginning of each experiment. The stack and tubing is also filled with 0.5 molal NaCl solution and the amount of solution inside is carefully measured. Salt solutions are pumped with a velocity of 35 ml min^{-1} and rinse solution is pumped at a velocity of 255 ml min^{-1}. Once electrical current is applied across the RED/ED stack, mass and conductivities of the solutions are logged. During the charging experiment, one solution gets diluted and the other concentrated. Once the diluate reaches below 0.01 molal, the experiment is considered finished. Data analysis of the ED experiments found that a current density of −32.5 A m^{-2} gives a high charge efficiency. At the end of this experiment the masses and concentrations of both solutions in the bottles and inside the tubing and stack are measured. These masses and concentrations serve as a starting point to perform RED experiments. In total, five RED experiments are performed at 40 °C with current densities ranging from 7.5 A m^{-2} to 37.5 A m^{-2} with steps of 7.5 A m^{-2}. The starting concentrations are 0.02 and 0.85 molal for the diluate and concentrate respectively. The RED experiments are considered finished when the measured voltage reaches zero. Data analysis of the RED experiments identifies 15 A m^{-2} to be the current density close to the optimal discharge efficiency. For both selected current densities (−32.5 and 15 A m^{-2}) the same experiments are repeated at 25 °C and 10 °C. The results are highly reproducible. For detailed information see the Supplementary Information for an example duplo experiment with a newly built stack. The standard average standard deviations for the individual datasets are: voltage, 0.01, mass, 0.23 and solution conductivity, 0.003.

3.3. Data analysis

Since the mass and concentrations of the solutions are known during operation of the CGFB, information about water mass change and salt content can be extracted at each time step. By dividing these mass transfers by the active ion-exchange membrane area of the stack, the water flux J_w and salt flux J_s is calculated. The flux of salt and water originates from the processes occurring inside the stack. Since the solutions take some time to travel from the bottle to the stack and back, these delays are carefully measured and taken into account by shifting the datasets appropriately to make sure that all readings (voltage, mass and conductivity) are well aligned. By doing so it is made sure that any measured mass change of the bottles caused by mass transports inside the RED/ED stack is properly linked.

4. Results and discussion

4.1. Energy capacity of and ideal CGFB

The energy content of an ideal CGFB during a full charge step is shown in Fig. 2. Since a concentration gradient flow battery is evaluated, the difference in concentration Δm (difference in molality) is a straightforward way for assessing the state of charge of the battery. When a battery is charged, a concentration gradient develops. Ideally, there would be only salt transport and no water transport. The stored Gibbs free energy of mixing ΔG_{mix} is shown at the y-axis of Fig. 2 and the concentration difference Δm is shown on the x-axis.

Interestingly, Fig. 2 shows that the majority of energy is stored at the end of the charging step. Halfway charging, at Δm = 0.5, only about 20% of the theoretical capacity is filled. In Section 4.2 the effect of the distribution of energy capacity with Δm on process performance is discussed in more detail.

4.2. Power dissipation as function of Δm during charge and discharge

With accurate measurements of mass transport, electrical current, cell voltage and theory given in Section 2 and Ref. [7], it is possible to calculate the instantaneous contribution of each major dissipation source and instantaneous (dis)charge efficiency of the process over full charge and discharge cycles.

Fig. 3A and B shows experimental results of a full charge (A) and discharge (B) step at currents densities of −32.5 A m^{-2} and 15 A m^{-2} at 40 °C. The y-axis shows the power lost or gained expressed in power per square meter of membrane area. For easy comparison the power values at charge mode are expressed as positive values.

Power lost as a result of internal resistance R_{int} is represented by the black curve [Ω]. At the end of a charge step, Δm is high and the fresh water becomes strongly diluted. As a result, internal resistance of the diluate compartment increases rapidly and explains the steep increase of [Ω] at high Δm (see annotation (***)).

The curve showing power lost by co-ion transport and internal

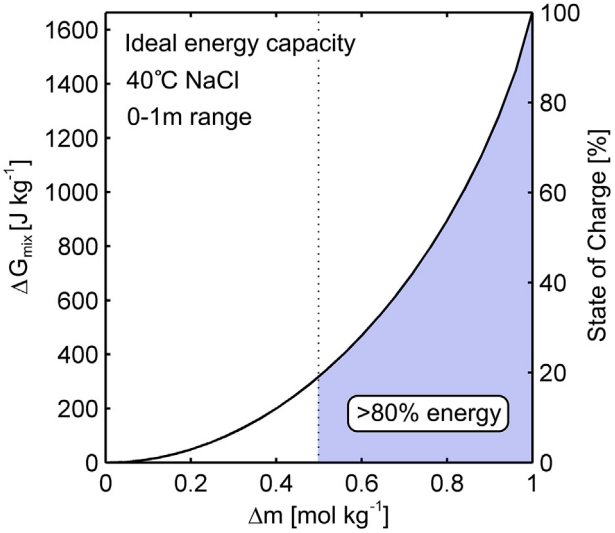

Fig. 2. Energy density of an ideal CGFB battery. Starting solutions are two solutions of 0.5 kg water and a concentration of 0.5 m NaCl. The left y-axis shows the total amount of Gibbs free energy of mixing (G_{mix}) stored in both solutions (J kg^{-1} solvent) as function of Δm. The right y-axis shows the state of charge (SoC) that is expressed as a percentage of the maximum amount of energy stored in the battery.

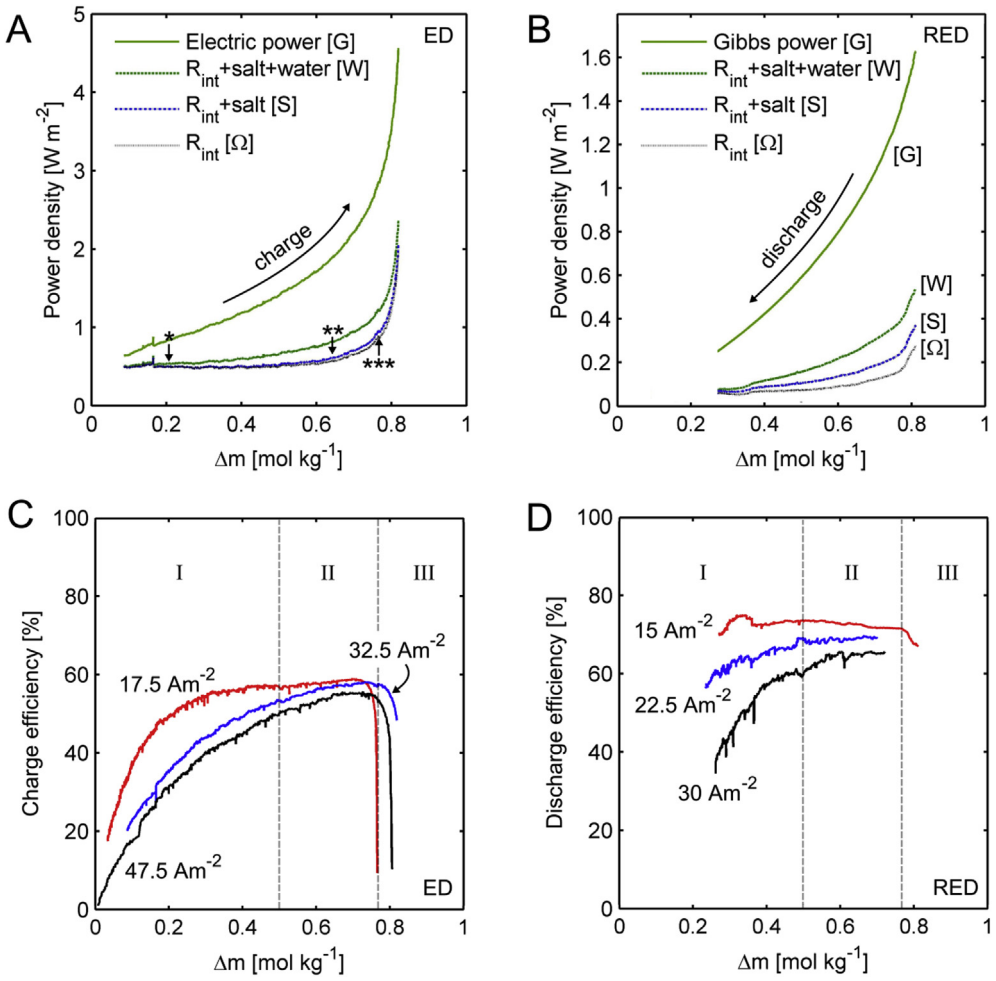

Fig. 3. A and B. Experimental results of a full charge (A) step at 32.5 A m^{-2} and discharge (B) step at 15 A m^{-2}. The x-axis shows the molality difference Δm and the y-axis the power lost or gained expressed in power per membrane area (W m^{-2}). R_{int} [Ω] shows the power lost as a result of internal resistance. The power lost by co-ion diffusion is given by the difference between the blue [S] and black [Ω] curve. Power loss caused by water transport is given by the difference between [W] and [S]. The difference between total spent electric power [G] and total dissipation losses [W] is the chemical power stored. For figure B the losses are described in the same manner as in A, except that [G] represents the total chemical power lost and the difference between [G] and [W] represents total electric power harvested. **C and D**. Figure C and D show the (dis)charge efficiency of charging and discharging at three current densities respectively. Also three zones are indicated by I-III. (For interpretation of the references to colour in this figure legend, the reader is referred to the web version of this article.)

resistance together [S] is plotted on top of the internal resistance curve [Ω]. The difference between [S] and [Ω] is the power lost by co-ion transport only. With increasing Δm, co-ion transport increases because of diffusion and this causes additional power loss. At annotation (**) the increasing power loss due to co-ion transport becomes visible.

Power loss caused by water transport is given by the difference between curve [W] and [S]. In charging (ED) mode, both osmosis and electro-osmosis cause water transport power losses whereas in discharging (RED) mode the electro-osmosis counteracts part of the power loss caused by osmosis (also refer to Section 2.2). Therefore, power loss by water transport is always higher during charging then during discharging. The effect of increasing power loss due to increasing osmosis with increasing Δm is clearly visible in Fig. 3A and B. Annotation (*) indicates where power loss by water transport becomes visible for the charging step. Osmosis is also responsible for the fact that a GCFB does not reach a Δm of 1. This is because the concentrate solution is being diluted.

During charging, the total electric power which is fed into the battery is given by curve [G]. The difference between curve [G] and the curve combining all losses [W] is the power actually stored as chemical energy. During discharge, the total chemical power released by mixing is given by curve [G]. Here, the difference between curve [G] and the curve combining all losses [W] is the power actually harvested as electric power.

4.3. Charge efficiency and discharge efficiency as function of Δm

The ratios of chemical power stored over electric power spent (ED mode) or electric power harvested over chemical power spent (RED mode) determine the (dis)charge efficiency of the CGFB (also refer to Eqs. (8) and (9)). Fig. 3C and D shows (dis)charge efficiencies for three selected current densities for both charge (3C) and discharge (3D).

All curves in Fig. 3C have the same shape. First efficiency increases steeply (zone I) followed by a region where efficiency levels off and reaches its maximum (zone II). At the end efficiencies drop rapidly (zone III).

The increase of efficiency in zone I is explained by the fact that the chemical energy stored per ion transported increases with increasing Δm (Fig. 2) while total power losses [W] stay relatively constant in zone I (Fig. 3A). In zone II, losses by osmosis and internal

resistance start to increase and therefore efficiency levels off. Finally, in zone III, losses caused by the internal resistance of the diluted solution cause a rapid decline in efficiency.

At the moment it is not smart to operate a CGFB in zone III. However, since power density and energy capacity in zone III are highest, it might be promising to decrease the resistance in this zone. Increasing the conductivity of the diluate compartment by introducing conductive spacers as described in Refs. [27,28], could be an example for making this zone accessible to the GCFB, leading improved efficiency and higher power densities.

Because internal resistance is the largest contributor to power losses in all zones, it has a strong effect on charge efficiency. As a consequence, efficiencies should increase if power loss by internal resistance is reduced. This is exactly what happens in Fig. 3C where lower current densities show higher efficiencies.

Power dissipation (Fig. 3B) during the discharge step and discharge efficiency (Fig. 3D) show identical behavior to the charge step. The charge and discharge step share the same zones.

From Fig. 3C and D it becomes clear that it is not smart to completely discharge a GCFB, since the charge efficiency is very low at low Δm. Also the power density of discharging is low in this region and so is the energy capacity. From Figs. 2, 3C and 3D it becomes clear that discharging beyond Δm of 0.5 m (zone I) is not efficient. Also note that operating the battery in zone III is not efficient either. Therefore, in practice a CGFB should be operated in zone II (working domain) to ensure the best performance. The working domain defined is this paper starts above Δm of 0.5 m and ends when the charge efficiency drops below 40%. It is important to note that pumping losses are not included in Fig. 3.

4.4. Effect of current density on power dissipation and (dis)charge efficiency

Next to a change of Δm, also current density has an effect on power dissipation and (dis)charge efficiency.

Fig. 4 shows experimental results of the working domain (see Section 4.3) of constant current experiments performed at 40 °C. The bottom dark-blue bars show the amount of chemical power stored (ED) and electric power extracted (RED). During charge mode, increasing current densities lead to more counter ions being transported, which in turn lead to a higher chemical power stored. During discharge mode, increasing discharge current densities also lead to increased counter ions transport, yielding higher electric power output.

Power dissipation due to water transport shows an interesting behavior. At low current densities, the battery is slowly charged or discharged. This means that at lower current densities, the solutions have to be recycled through the stack more often. As a result the average time the solution spents inside the stack increases over a full charge/discharge cycle. An increase in (dis)charge time leads to increased water transport due to osmosis. Therefore, decreasing current densities cause a relative increase in power loss due to water transport.

Different from osmosis, electro-osmosis is coupled to the direction and size of the salt transport. For ED, electro-osmosis causes additional power losses. An increasing current density during charging therefore yields higher power losses by electro-osmosis. For RED, the opposite occurs and electro-osmosis decreases power losses. With increasing current, net water transport is reduced to almost zero at 37.5 A m^{-2}. The effect of electro-osmosis on power dissipation by water transport as function of current density is very similar to the previous study [7] and is also predicted by data from Veerman et al. [29].

Power lost by unwanted salt transport seems limited over the whole range of current densities and can be considered as the dissipation factor of least importance in a GCFB. The same result was previously reported in Refs. [6,7]. The low co-ion transport can be explained by the high charge selectivity of the membranes in the concentration range used. With increasing current densities the total power dissipation by internal resistance increases rapidly (Ohm's law).

In Fig. 4 also the average (dis)charge efficiency of the whole charge (ED) and discharge (RED) step inside the working domain is shown on the right y-axis. Two observations can be made: (i) Although two optima can be observed, the efficiency remains rather constant over the whole range of current densities tested. (ii) Discharge efficiencies are generally higher than charge efficiencies.

The first observation can be explained by the fact that power loss due to internal resistance is traded off by the power loss due to water transport. At low current densities, osmosis is high because of the longer (dis)charge time and internal resistance losses are low. At higher current densities, osmosis is decreased because of a reduced (dis)charge time but internal resistance losses are high. This trade-off effect is only valid at low current densities reported in this study. Since power losses by osmosis are linearly related to (dis)charge time (and thus current density) but power losses by internal resistance are related to the current density squared, at higher currents power dissipation by internal resistance will

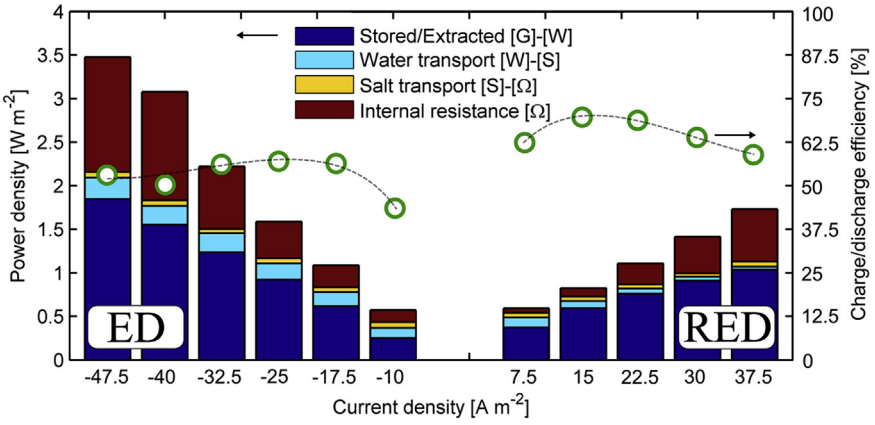

Fig. 4. Experimental results of power density and (dis)charge efficiency as function of current density measured at 40 °C. The x-axis shows the current density where negative current density is charge (ED) and positive current density is discharge (RED). The left y-axis shows the measured power dissipation contribution for each dissipation source plus the power stored (ED) or extracted (RED). The right y-axis shows the (dis)charge efficiency of the charge/discharge process. All values are averages from all values measured inside the working domain of each experiment (see Section 4.3, Δm > 0.5 and η > 40%). Dotted lines are for guiding the eye. The size of the dots is chosen for clarity. (For interpretation of the references to colour in this figure legend, the reader is referred to the web version of this article.)

increase rapidly and (dis)charge efficiencies will decrease rapidly.

The second observation is explained by the fact that electro-osmosis is energetically favourable for the discharge step but energetically unfavourable during the charge step. It is also observed that the internal resistance losses for charging are somewhat higher compared to discharging, which can be explained by concentration polarization at the membrane interface. In addition, co-ion transport (and thus the associated power loss) is typically lower with discharging than with charging because of the difference in the direction of the electric field [7].

4.5. Effect of temperature on dissipation and (dis)charge efficiency

Earlier studies showed the effect of temperature on either RED or ED considering the internal resistance and mass transport [15–21]. To study the effect of temperature on power dissipation and (dis)charge efficiency under GCFB operating conditions several experiments at different temperatures have been performed.

Fig. 5 shows that for identical current densities and for increasing temperature, power losses decrease due to internal resistance (for charging from 1.41 to 0.72 W m^{-2} and for discharging from 0.22 to 0.10 W m^{-2}). For RED this is also reported by Ref. [15] and for ED by for example [16,20]. The decreased internal resistance makes it possible to operate at higher currents and therefore at higher power densities. However, water transport also increases with increasing temperature (for charging from 0.12 to 0.22 W m^{-2} and for discharging from 0.01 to 0.08 W m^{-2}). Fig. 5 shows how a decrease in power losses by internal resistance is partly counteracted by increased osmosis. In fact, water transport turns out to be of such importance that it has been given special attention and is discussed in separate Section 4.6.

Power losses due to unwanted salt transport ('salt' in Fig. 5) are very small relative to other losses. However, co-ion transport does increase with increasing temperature as can be seen in Fig. 5. This increase in co-ion transport is in line with results from Refs. [15,17]. Since the power losses due to co-ion transport are so small compared to other types of losses, it is considered not to be a factor prohibiting the use of higher operating temperatures.

4.6. Water transport

Performance of a GCFB is seriously hampered by water transport. Therefore, the effect of water transport over full charge/discharge cycles and the effect of temperature on water transport are discussed in this section in more detail.

Fig. 6 shows how the concentrations in both reservoirs develop during a full charge (red markers) and discharge (green markers) cycle. In addition, the ideal battery presented in Section 4.1 is depicted in Fig. 6 to clearly indicate mismatch between ideal and real situation. Theoretically the battery could be charged until ~1650 J kg^{-1} (top purple marker Fig. 6), whereas experimentally only ~1050 J kg^{-1} is achieved. The reason for this is that water is transported from the diluate to the concentrate reservoir during the entire charge step. As a result the concentrate gets diluted (right top panel) and the maximum Δm that can be reached in practice is lower than the ideal value. Next to the limited Δm, energy density is also limited because of an unfavourable mixing ratio between fresh and salt water. In the previous work, see Ref. [7], it is shown that at high energy density, it is favourable to have a bit more fresh water then salt water. Water transport causes the opposite to happen and therefore energy density becomes limited.

Panel C shows water transport in detail. When charging, the mass of water in the concentrate reservoir (y-axis) increases and the mass of the diluate decreases. The increased water transport towards the end of the charge step is caused by the increased concentration difference. When discharging, water again is transported from diluate to concentrate but since electro-osmosis takes place opposite to osmosis, total water transport is lower. The situation is slightly different during discharge, where Δm decreases and osmosis decreases gradually, but since electro-osmosis stays constant, overall water transport becomes near zero or negative at the end of the discharge step. After a full charge/discharge cycle the water transported has caused hysteresis and the battery needs to be restored. The most straightforward way would be to replace the lost volume of fresh water with water from the concentrate. If the CGFB is completely discharged and both solutions have the same concentration, this would not lead to extra energy dissipation. However, completely discharging a CGFB was shown inefficient. If therefore discharge is stopped before the battery enters zone I, there still is a difference in concentration. Transferring part of the concentrate to the diluate would lead to undesired mixing yielding some additional energy dissipation (in the particular case of Fig. 6, equalizing the water masses would yield a Gibbs free energy loss of ~131 J kg^{-1}). The hysteresis issue of a CGFB remains to be solved to make the battery more energy efficient.

Fig. 5 also shows that water transport is affected by

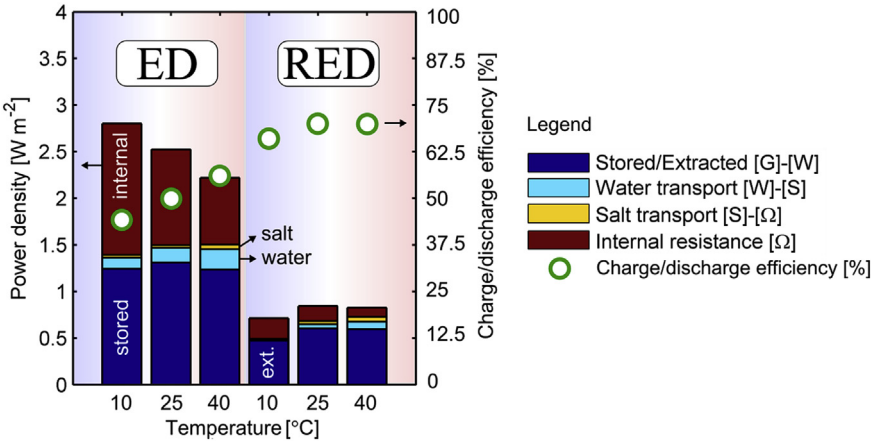

Fig. 5. Experimental results of power dissipation and (dis)charge efficiency of a GCFB at different temperatures. Charge experiments are done at a current density of −32.5 A m^{-2} (ED) and discharge at 15 A m^{-2} (RED). The x-axis shows the temperatures. The left y-axis shows the measured power dissipation contribution for each dissipation source plus the power stored (ED) or extracted (RED). The right y-axis shows the (dis)charge efficiency of the charge/discharge process. All values are averages from all values measured inside the working domain of each experiment (see Section 4.3). The size of the dots is chosen for clarity. (For interpretation of the references to colour in this figure legend, the reader is referred to the web version of this article.)

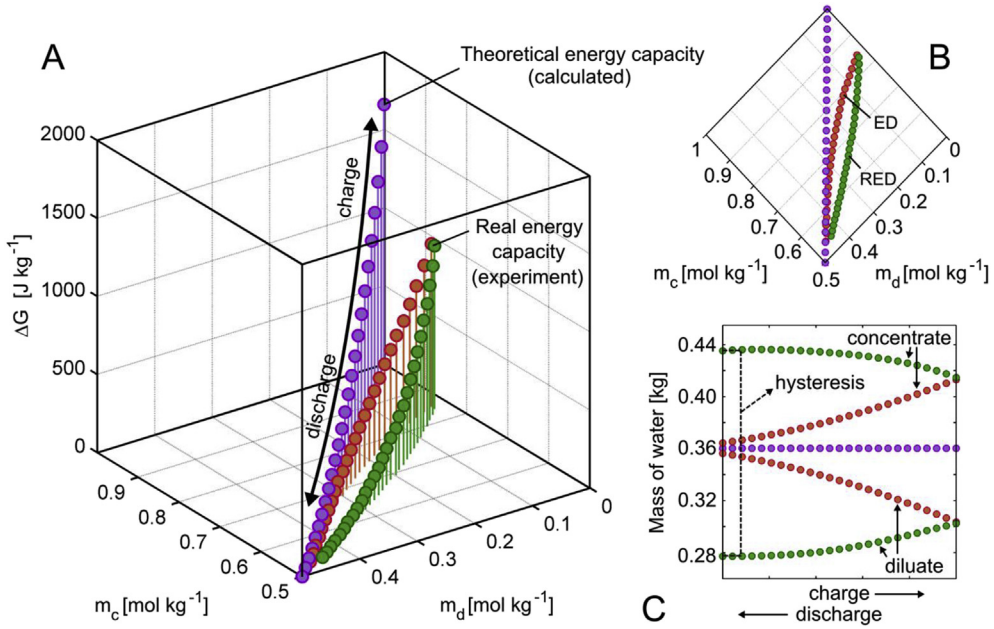

Fig. 6. Stem plot of the energy density of an ideal battery (purple markers) and the energy density of a real battery during charge (red markers) and discharge (green markers) at 40 °C. **A**: On the x and y-axis the solution molalities of both reservoirs are shown. The z-axis represents the Gibbs energy stored at that instant in J kg^{-1} of water in the system. **B**: Top view of panel A is given in panel B, to clearly show the deviation from the ideal battery (purple markers). **C**: Panel C shows the mass of water in each reservoir during an ideal charge and discharge cycle (purple markers) and of the measured charge (red markers) and discharge (green markers) cycle. The difference of water mass at the end of each cycle is "hysteresis" of the battery which is responsible for decrease of energy density of the CGFB. (For interpretation of the references to colour in this figure legend, the reader is referred to the web version of this article.)

temperature. To see how osmosis and electro-osmosis are separately affected by temperature, Eq. (5) and the regression procedure used in Ref. [7] are used to quantify this effect on the hydraulic permeability constant L_p and the water transport number t_w, see Table 1.

Table 1 shows that the experimental data can be fitted very well ($R^2 \geq 0.998$) with Eq. (5). This indicates that Eq. (5) is very well able to quantitatively describe water transport over complete charge/discharge cycles at several temperatures. In addition, the hydraulic permeability constant increases with temperature. This was expected since Fig. 5 already showed that power losses caused by water transport increased with increasing temperature. Surprisingly, the water transport number stays nearly constant over the whole temperature range indicating that electro-osmosis is hardly affected by temperature. To improve battery performance regarding water transport, membranes with lower hydraulic permeability are needed to decrease hysteresis, increase energy capacity and (dis)charge efficiency.

5. Conclusions

Full charge and discharge cycles of a CGFB have been performed experimentally at 40 °C with current densities ranging from −47.5 A m^{-2} (ED) to 37.5 A m^{-2} (RED). In addition, full charge (−32.5 A m^{-2}) and discharge (15 A m^{-2}) cycles have been performed at 10 °C and 25 °C. Dissipation of energy and (dis)charge efficiency for both changing concentrations (0–1 mol NaCl kg^{-1} H_2O) and temperatures is investigated and discussed.

The majority of the energy is stored at the end of the charge step where the difference in molality is greatest and the diluate very fresh. With increasing molality difference, power losses by osmosis and co-ion transport increase. In contrary power losses due to internal resistance are shown to be relatively constant over the whole range of molality differences, except for the highest molality difference due to high resistance of the diluate solution. Considering the (dis)charge efficiency, three zones can be distinguished over a typical charge and discharge cycle. The first zone (0–0.5 Δm) is characterized by low (dis)charge efficiency because of a small amount of energy being stored or extracted in this range, while power losses due to internal resistance are significant. The second zone, (~0.5–0.75 Δm), has the highest (dis)charge efficiency and is considered the most optimal working domain of a real GCFB. In this zone, osmosis and co-ion transport are modest, while chemical power stored or electric power extracted is high. The last zone, (~>0.75 Δm), is characterized by the highest amount of chemical power stored or electric power extracted, but because of significant osmosis, co-ion transport and high internal resistance it is not the most optimal operational zone for the CGFB.

Power loss by co-ion transport is typically limited to a few percent in comparison to other losses. This can be explained by the high selectivity of the membranes in the chosen concentration range. Co-ion transport is shown to increase with increasing temperature but remains very small. Power loss by co-ion transport is therefore considered the least important dissipation factor of a GCFB.

The averaged (dis)charge efficiency of the GCFB in the working domain is shown to be quite stable over all current densities applied. This is explained by the trade-off of power dissipation

Table 1
Estimated parameters L_p and t_w by regression analysis of experimental data. The data includes both ED and RED operating modes at several temperatures.

T (°C)	Parameter	Unit	Value	R^2
10	L_p	kg m^{-2} s^{-1} kg J^{-1}	5.5e-09	0.998
	t_w	mol H_2O mol^{-1} salt	8.6	
25	L_p		8.9e-09	1
	t_w		8.2	
40	L_p		1.4e-08	1
	t_w		8.0	

occurring between water transport and internal resistance. For high current densities power dissipation by internal resistance is high, but since total charge and discharge times are shorter, osmosis losses are lower. For low current densities the opposite is true, with low power losses due to internal resistance but higher power losses due to osmosis. Two optima can be distinguished, for ED the maximum charge efficiency measured is 58% at a current density of 25 A m^{-2} and for RED 72% at 15 A m^{-2} yielding a round trip efficiency of about 42%. The highest temperature recorded the highest (dis)charge efficiencies. This is explained by the low internal resistance at higher temperatures. However the increase in (dis)charge efficiency is limited since also water transport is shown to increase with temperature.

Water transport does triple damage to the GCFB; it leads to a lower energy capacity, a lower (dis)charge efficiency and causes hysteresis. Regression analysis on measured water transport of multiple charge/discharge cycles shows that with higher temperatures the hydraulic permeability of the membranes increases and electro-osmosis stays unaffected. Just as in the previous study [7], even with higher temperatures, power losses due to internal resistance remain the most important dissipation factor in a GCFB and in this regard significant improvement of membranes is needed.

Acknowledgements

This work was performed in the cooperation framework of Wetsus, European Centre of Excellence for Sustainable Water Technology (www.wetsus.nl). Wetsus is co-funded by the Dutch Ministry of Economic Affairs and Ministry of Infrastructure and Environment, the Province of Fryslân and the Northern Netherlands Provinces. The authors like to thank the participants of the research theme “Blue Energy” for the fruitful discussions and their financial support. In addition the authors would like to thank Slawomir Porada for the valuable discussions.

Appendix A. Supplementary data

Supplementary data related to this article can be found at http://dx.doi.org/10.1016/j.jpowsour.2016.11.043.

References

[1] A. Sternberg, A. Bardow, Power-to-what? - environmental assessment of energy storage systems, Energy Environ. Sci. 8 (2015) 389–400.
[2] M. Carbajales-Dale, C.J. Barnhart, S.M. Benson, Can we afford storage? A dynamic net energy analysis of renewable electricity generation supported by energy storage, Energy Environ. Sci. 7 (2014) 1538–1544.
[3] B. Dunn, H. Kamath, J.-M. Tarascon, Electrical energy storage for the grid: a battery of choices, Science 334 (November 18, 2011) 928–935.
[4] S. Corcuera, J. Estornés, C. Menictas, Chapter 2-Economics of batteries for medium- and large-scale energy storage, in: C.M.S.-K.M. Lim (Ed.), Advances in Batteries for Medium and Large-scale Energy Storage, Woodhead Publishing, 2015, pp. 29–53.
[5] M. Beaudin, H. Zareipour, A. Schellenberglabe, W. Rosehart, Energy storage for mitigating the variability of renewable electricity sources: an updated review, Energy Sustain. Dev. 14 (12//2010) 302–314.
[6] R.S. Kingsbury, K. Chu, O. Coronell, Energy storage by reversible electrodialysis: the concentration battery, J. Membr. Sci. 495 (1 dec. 2015) 502–516, http://dx.doi.org/10.1016/j.memsci.2015.06.050.
[7] W.J. van Egmond, M. Saakes, S. Porada, T. Meuwissen, C.J.N. Buisman, H.V.M. Hamelers, The concentration gradient flow battery as electricity storage system: technology potential and energy dissipation, J. Power Sources 325 (9/1/2016) 129–139.
[8] H. Strathmann, Electrodialysis, a mature technology with a multitude of new applications, Desalination 264 (12/31/2010) 268–288.
[9] T. Xu, C. Huang, Electrodialysis-based separation technologies: a critical review, AIChE J. 54 (2008) 3147–3159.
[10] A.H. Galama, M. Saakes, H. Bruning, H.H.M. Rijnaarts, J.W. Post, Seawater predesalination with electrodialysis, Desalination 342 (2014) 61–69.
[11] A.H. Galama, G. Daubaras, O.S. Burheim, H.H.M. Rijnaarts, J.W. Post, Fractioning electrodialysis: a current induced ion exchange process, Electrochim. Acta 136 (2014) 257–265.
[12] D.A. Vermaas, M. Saakes, K. Nijmeijer, Doubled power density from salinity gradients at reduced intermembrane distance, Environ. Sci. Technol. 45 (2011/08/15) 7089–7095.
[13] N.Y. Yip, D.A. Vermaas, K. Nijmeijer, M. Elimelech, Thermodynamic, energy efficiency, and power density analysis of reverse electrodialysis power generation with natural salinity gradients, Environ. Sci. Technol. 48 (2014) 4925–4936.
[14] J. Veerman, M. Saakes, S.J. Metz, G.J. Harmsen, Reverse electrodialysis: evaluation of suitable electrode systems, J. Appl. Electrochem. 40 (2010/08/01) 1461–1474.
[15] A. Daniilidis, D.A. Vermaas, R. Herber, K. Nijmeijer, Experimentally obtainable energy from mixing river water, seawater or brines with reverse electrodialysis, Renew. Energy 64 (4//2014) 123–131.
[16] T. Bejerano, C. Forgacs, J. Rabinowitz, Further developments in the high temperature electrodialysis, Desalination 3 (1967) 129–134.
[17] F.Q. Mir, A. Shukla, Sharp decline in counter-ion transport number of electrodialysis ion exchange membrane on moderate increase in temperature, Desalination 372 (9/15/2015) 1–6.
[18] V.N. Smagin, N.N. Zhurov, D.A. Yaroshevsky, O.Y. Yevdokimov, Optimization of electrodialysis process at elevated temperatures, Desalination 46 (5//1983) 253–262.
[19] W.A. McRae, W. Glass, F.B. Leitz, J.T. Clarke, S.S. Alexander, Recent developments in electrodialysis at elevated temperatures, Desalination 4 (1968) 236–247.
[20] C. Forgacs, L. Koslowsky, J. Rabinowitz, The desalination of sea water by high temperature electrodialysis, Desalination 5 (1968) 349–358.
[21] F.B. Leitz, M.A. Accomazzo, W.A. McRae, High temperature electrodialysis, Desalination 14 (2//1974) 33–41.
[22] K.S. Pitzer, G. Mayorga, Thermodynamics of electrolytes. II. Activity and osmotic coefficients for strong electrolytes with one or both ions univalent, J. Phys. Chem. 77 (1973/09/01) 2300–2308.
[23] L. Silvester, K. Pitzer, Thermodynamics of electrolytes (VIII)-high-temperature properties, including enthalpy and heat capacity, with application to sodium chloride, J. Phys. Chem. 81 (1977) 1822–1828.
[24] M. Tedesco, A. Cipollina, A. Tamburini, I.D.L. Bogle, G. Micale, A simulation tool for analysis and design of reverse electrodialysis using concentrated brines, Chem. Eng. Res. Des. 93 (1//2015) 441–456.
[25] J. Veerman, M. Saakes, S. Metz, G. Harmsen, Reverse electrodialysis: a validated process model for design and optimization, Chem. Eng. J. 166 (2011) 256–268.
[26] J. Veerman, M. Saakes, S. Metz, G. Harmsen, Reverse electrodialysis: performance of a stack with 50 cells on the mixing of sea and river water, J. Membr. Sci. 327 (2009) 136–144.
[27] V.K. Shahi, S. Thampy, R. Rangarajan, The effect of conducting spacers on transport properties of ion-exchange membranes in electrodriven separation, Desalination 133 (2001) 245–258.
[28] P. Długołęcki, J. Dąbrowska, K. Nijmeijer, M. Wessling, Ion conductive spacers for increased power generation in reverse electrodialysis, J. Membr. Sci. 347 (2010) 101–107.
[29] J. Veerman, R. De Jong, M. Saakes, S. Metz, G. Harmsen, Reverse electrodialysis: comparison of six commercial membrane pairs on the thermodynamic efficiency and power density, J. Membr. Sci. 343 (2009) 7–15.